Polarization-insensitive, wide-angle broadband perfect absorber with patch structures

BEIBEI WU[a], JIANGUO WANG[b,*]

[a]*College of Mathematics and Physics, Shanghai University of Electric Power, Shanghai 200090, China*
[b]*Laboratory of Thin Film Optics, Shanghai Institute of Optics and Fine Mechanics, Chinese Academy of Sciences, Shanghai 201800, China*

We present a polarization-insensitive, wide-angle broadband perfect absorber with planar patch structures. The finite difference time domain method, transfer matrix method, and effective medium theory are applied for the design and analysis of the perfect absorber. Titanium nitride (TiN) and indium tin oxide (ITO) are introduced as the layers and planar patch structures. The unit cell structure is mainly composed of a pair of TiN/ITO layers and four planar patches as the top layer. The average absorption is higher than 95% between the wavelengths of 550 and 1100 nm. The average absorption remains above 90% between 500 nm and 1100 nm with a wide range of incident angles from 0° to 60°. The electrical field intensity distributions are calculated to understand the broadband absorption mechanism. The designed broadband absorber could be very promising for application in solar thermal energy harvesting and photo detection devices.

1. Introduction

Metamaterials are typically composed of two structured metallic layers separated by a dielectric spacer, in which the electric and magnetic responses can be appropriately tuned by tailoring the structure. Metamaterial absorption is one of the interesting properties in artificially engineered metamaterials [1-8]. Metamaterial absorbers based on structures consisting of metal-dielectric-metal thin films have been widely applied to the perfect absorber design [9, 10]. Plasmonic absorption in Au and Ag, also called localized surface plasmonic resonance, has been extensively investigated [11-14]. Many efforts have been made to achieve metamaterial perfect absorbers with polarization insensitive, wide-angle, multi-band or broadband performance from the terahertz to optical range. These properties can be potentially applied in devices such as photodetectors [15], sensors [16], and photovoltaic solar cells [17].

Aydin *et al.* demonstrated an absorber that yields broadband and polarization-independent resonant light absorption over the entire visible spectrum (400-700nm) with an average measured absorption of 0.71 [13]. Hyungduk Ko proposed a broadband visible light absorber composed of multiple metal-dielectric-metal layers with an average simulated absorption of 93% over the entire visible spectrum of 400-700 nm by controlling the geometric parameters [14]. Cui *et al.* [18] proposed an ultra-broadband and wide-angle thin film absorber based on an anisotropic metamaterial. Nielsen *et al.* [19] demonstrated a periodic array of differently sized and circular gap plasmonic resonators in the entire visible wavelength range. Song *et al.* [20] proposed a light harvesting system by combining a broadband absorber with a perfect selective emitter on the opposite surface separated by a tungsten cylinder on a silica substrate. Semiconductor based oxides and transition-metal nitrides have been proposed as alternative plasmonic materials [21-23]. The semiconducting oxides have low loss in the near-IR range and metal nitrides serve as alternatives to gold and silver in the visible frequencies. A broadband metamaterial absorber with a square ring structure had been reported by *Li et al.* [24]. A theoretical perfect absorber with a TiN nano-disk array was proposed by Wang *et al.* [25], and numerical simulations indicated that the absorber could exhibit an average absorbance larger than 99% from 560 to 675 nm. Transparent conducting oxides have been widely used in optoelectronic devices. Indium tin oxide (ITO) provides wide opportunities for realizing surface plasmon polariton (SPP) excitations in the IR region [26, 27]. In this work, titanium nitride and indium tin oxide thin films are introduced as the layers and planar patch structure. The broadband, polarization insensitive, and wide angle metamaterial absorber with patch structures is investigated using finite difference time domain (FDTD) simulation, the transfer matrix method, and effective medium theory.

2. Structural model and simulations

The schematic of the unit cell of the proposed broadband absorber is shown in Fig. 1. The absorber is composed of three layers, a top layer with four patches, a spacer layer, and a bottom layer. The structural parameters are denoted as follows: p is the pitch length of the square unit cell and t_1, t_2, t_3 and t_4 are the thicknesses of the TiN patch layer, ITO spacer layer, TiN bottom layer, and substrate, respectively. BK7 glass is employed as the device substrate.
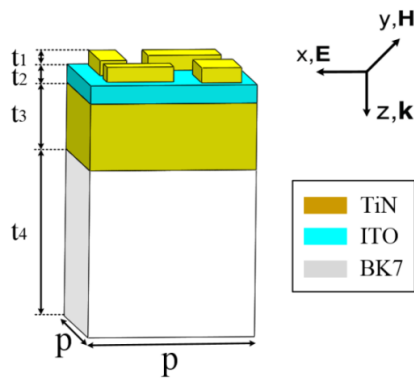
Fig. 1. Schematic of the unit cell of the proposed broadband absorber; the overall structure is a periodic array of the unit cell

The finite difference time domain method [28, 29] is used for the numerical simulation of the plasmonic absorption performance. The dielectric functions and optical constants are obtained from Refs. [30] and [31]. The plane wave is incident on the absorber along the z direction, the x and y directions have Bloch's boundary conditions, and the z direction has a perfectly matched layer in this simulation. The p-polarization plane is parallel to x-z plane, and the s-polarization plane is parallel to y-z plane. The interface between the TiN layer and BK7 substrate is defined as x-y plane ($z = 0$). The reflection (R) was detected with a power monitor located behind the radiation source of the plane waves, and the transmission (T) was detected with a power monitor located at −50 nm relative to the bottom of the base TiN layer. The gap between the light source and the base TiN layer is 1.4 μm, and the gap between the reflection monitor and the bottom of the base TiN layer is 1.5 μm. The absorbance spectrum $A(\lambda)$ can be calculated from the corresponding reflection spectrum $R(\lambda)$ and transmission spectrum $T(\lambda)$ using the relationship, $A(\lambda) = 1 - R(\lambda) - T(\lambda)$.
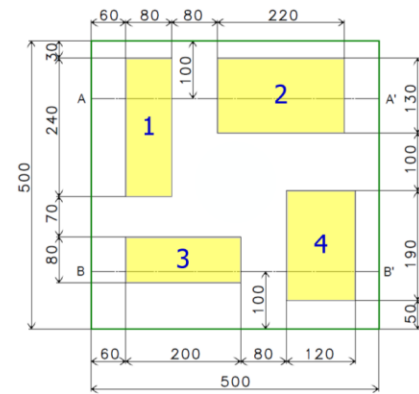
Fig. 2. Schematic of the four patch structured perfect absorber. All dimensions shown in the diagram are in nm

In the numerical simulation, the dimensions of the unit elements are defined as follows: t_1=45nm, t_2=55nm, t_3=200 nm and t_4=20 μm. The dimensions of the four patches (patch 1, patch 2, patch 3, and patch 4) in the x-y plane are also shown in Fig. 2. The blocks in yellow are the patches with TiN material. The width and length of patch 1 are 80 nm and 240 nm, respectively. The width and length of patch 2 are 220 nm and 130 nm, respectively. The width and length of patch 3 are 200 nm and 80 nm, respectively. The width and length of patch 4 are 120 nm and 190 nm, respectively. The pitch of the unit cell is 500 nm. The other dimensions are the relative position distribution of the four patches in the unit cell. The cross sectional planes AA' and BB' are perpendicular to the x-y plane and run across AA' and BB' lines, respectively. The distance between the AA' or BB' and the edge of the unit cell is 100 nm. In all numerical simulations, a cubic mesh with a size of 2.5 nm was employed.

3. Results and discussions

The resonant absorbance properties in metamaterial have been investigated by different groups [32-34]. There are two different but concomitant mechanisms responsible for the resonant absorption. One is the excitation of SPPs, which is the direct result of the periodical arrangement of the sub-wavelength structure. SPPs are based on the interference of multiple waves scattered by the microstructure array and can obviously be affected by the properties of the arrangement and thickness of the spacer layer. The other mechanism involves localized surface plasmon resonances (LSPR), as either localized modes or localized waveguide resonances, mostly due to the shape and size of the microstructure array. The proposed broadband perfect absorber is based on two planar layers and one layer with four patches. The bottom TiN layer acts as an optical mirror to block the transmittance of the incident light. The top patch layer scatters electromagnetic waves and excites SPPs and LSPRs. The coupling between the top and bottom layers results in magnetic resonance,

depending on the dielectric constants of the middle spacer layer.

The absorption spectrum with four patches and each of the single patches are shown in Fig. 3(a). The resonance absorption bandwidth with each single patch is narrow. The resonant spectrum of each patch has two resonance peaks. However, the resonant spectra of all four patches have the same peak at $\lambda_0 = 600$ nm. This absorption peak is a result of the SPP resonance. The LSPR resonant wavelengths are determined by the shapes of the patches. The incident plane wave excites different resonant wavelengths at $\lambda_1, \lambda_2, \lambda_3,$ and λ_4 for single patches 1, 2, 3, and 4, respectively. The resonant spectrum of the absorber with four patches finally merges into the broadband absorption spectrum of the perfect absorber due to the coupling between each resonant patch.
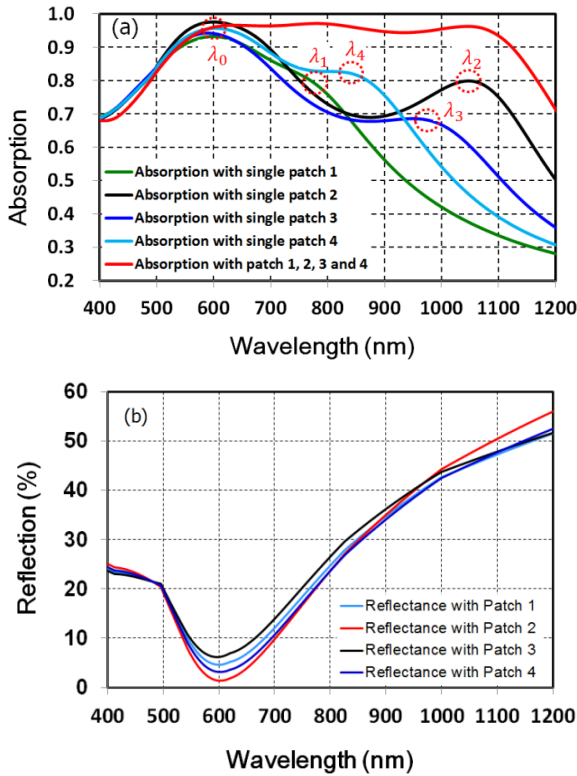
Fig. 3. (a) Numerical absorption spectra from FDTD method; (b) numerical reflective spectra of the absorbers from transfer matrix method and effective medium theory

To verify the impact of the patches on the optical transfer properties, the transfer matrix method and effective medium theory are used to calculate the reflection of the perfect absorber with the patches. The transfer matrix method uses the transfer matrices for wave propagation through the layers and at interfaces and provides an efficient toolbox for a wide variety of thin film optical problems [35]. The top layer with the patch is regarded as a layer with equivalent dielectric constants. Further, the optical constants of this equivalent layer are extracted with the effective medium theory [36]. The

dielectric function of the equivalent layer is defined by the following formula:

$$\varepsilon_{eff} = f_a\varepsilon_a + (1-f_a)\,\varepsilon_b \qquad (1)$$

and

$$1/\varepsilon_{eff} = f_a/\varepsilon_a + (1-f_a)/\varepsilon_b \qquad (2)$$

where, f_a is the volume fraction of material 'a' and ε_i (i=a, b, eff) are the dielectric constants for component 'a', component 'b', and the effective mixture, respectively. Here, material 'a' is TiN and material 'b' is air. The numerical reflective spectra of the absorbers obtained by the transfer matrix method and effective medium theory is shown Fig. 3(b). There is an antireflection valley at 600 nm, which is consistent with the result obtained by FDTD calculation (Fig. 3(a)).

In order to understand the absorption mechanism of this broadband absorber, we investigated the electrical intensity distribution at several selected wavelengths. Fig. 4 shows the electrical intensity distributions at two resonant wavelengths: $\lambda = 600$ nm and 1200 nm with normal incidence.
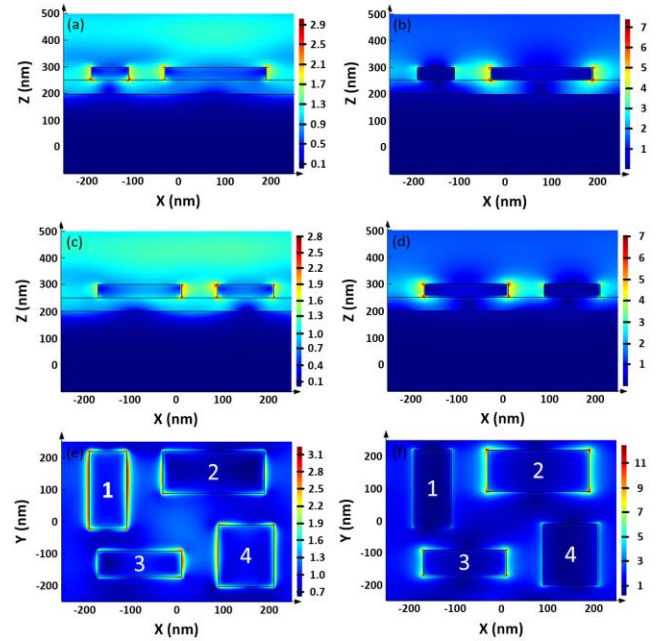
Fig. 4. Electrical intensity distribution of the broadband absorber for normal incidence of p-polarized light: (a) cross-section AA' with 600 nm light; (b) cross-section AA' with 1200 nm light; (c) cross-section BB' with 600 nm light; (d) cross-section BB' with 1200 nm light; (e) interface between the top patch layer and middle ITO layer with 600 nm light; (f) interface between the top patch layer and middle ITO layer with 1200 nm light

The electrical intensity distribution is shown in Fig. 4 for the cross-sections AA', BB' and the interface between the top patch layer and middle ITO layer using 600 nm and 1200 nm incident light. All four patches show a strong resonance at 600 nm. However, there are only two patches

(patch 2 and path 3) with a strong plasmonic resonance at 1200 nm. These results are consistent with those shown in Fig. 3. The strongest absorption occurs at 600 nm.

The diameter of the absorber is one of the critical parameters controlling light absorption. The electric and magnetic fields in the unit cells are strongly influenced by the dimensions of the absorber [14, 37]. For a further analysis of the mechanism of the proposed broadband perfect absorption, the absorption spectrum is calculated using three pitch values and the results are shown in Fig. 5. The absorption spectrum can be broadened when the pitch is increased from 450 to 550 nm. The absorption wavelength at 600 nm is maintained with no wavelength shift for the three pitch configurations. Further, the absorption strength decreases with the increment in pitch. It is mainly due to the SPPs in this wavelength range. The absorption shows a red shift in the long wavelength region, and the absorption strength becomes higher when the pitch is changed from 450 to 550 nm. There is an absorption peak at 1100 nm when the pitch is 550 nm. Moreover, the absorption spectrum can be adjusted by changing the geometrical parameters of the broadband perfect absorber. The absorption is higher than 95 % between 550 and 1100 nm when the pitch is 500 nm.
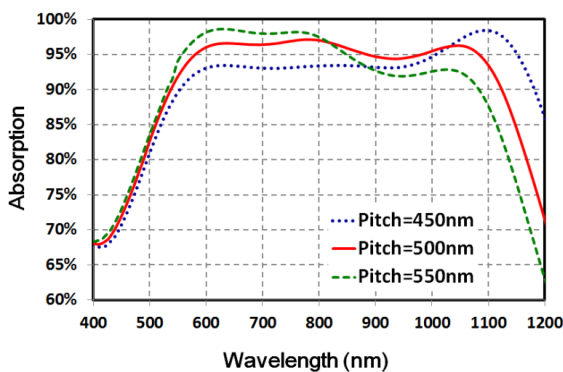
Fig. 5. Absorption spectra of the broadband absorbers with pitch values of 450 nm, 500 nm and 550 nm for normal incidence of light

In the previous analysis, the absorption was only investigated with normal incident light. However, the broadband absorption should be maintained for a wide range of incident angles for practical applications. The absorption spectrum as a function of the polarization angle is shown in Fig. 6 for the p-polarization incident light. For simplicity, only the results of the p-polarization incident light are shown because the result with s-polarization is similar.
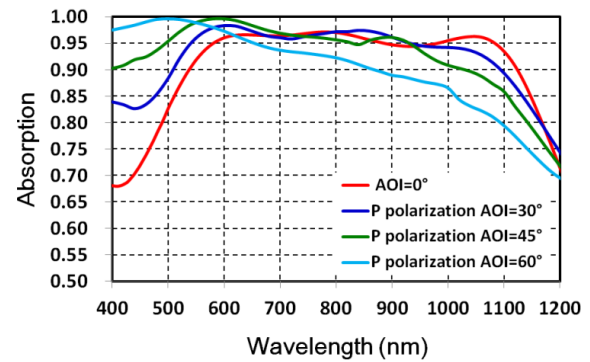
Fig. 6. Absorption for the absorber with 500 nm pitch for different angles of incidence with p-polarized incident light

Results show that the average absorption of the perfect absorber is higher than 95% from 0° to 45°. The electric field intensity plays an important role in driving the surface plasmonic resonance at the optical frequency. The SPPs and LSPRs coexist with the increase in the angle of incidence (AOI). The absorption spectrum shows a blue shift when AOI is increased, because of the effective thickness of the spacer layer. The absorption decreases at longer wavelengths because of the coupling between the top patch layer and the bottom TiN layer. The average absorption is maintained above 90% for 60° AOI. The electrical intensity of the broadband absorber cross-section AA' with 500 nm pitch under 600 nm incident light is shown in Fig. 7. The maximum peaks are 3.01, 3.74, 3.87, and 3.43 at 600 nm incident light for the four AOIs of 0°, 30°, 45°, and 60°, respectively. The strongest resonance occurs at 45° AOI, which is consistent with the absorption spectrum shown in Fig. 6. The result reveals that the proposed broadband perfect absorber has a wide-band and polarization-insensitive absorption over a wide range of incident angles.
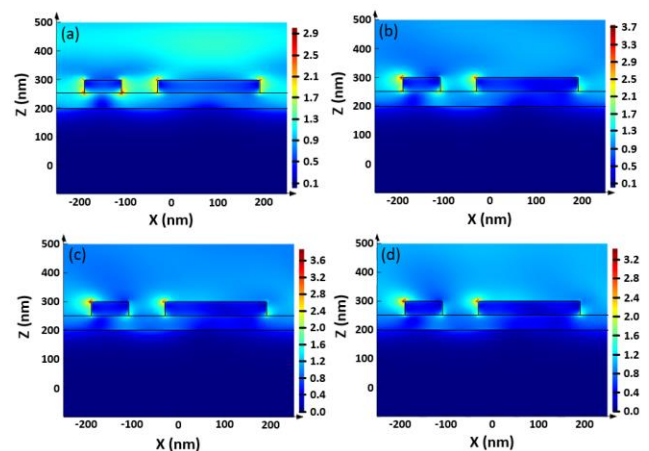
Fig. 7. Electrical intensity distribution of the broadband absorber cross-section AA' with 500 nm pitch using 600 nm incident light: (a) normal incidence; (b) 30° AOI; (c) 45° AOI; (d) 60° AOI

4. Conclusion

In conclusion, a polarization-insensitive broadband absorber with patch structures is proposed and its absorption is investigated numerically. The absorber exhibits wide-band perfect absorption characteristics. It has an average absorbance of 95% from 400 to 1200 nm under appropriate geometrical conditions. Furthermore, the electromagnetic field intensity distributions under different angles of incidence at two selected wavelengths are investigated to understand the broadband absorption mechanism. The periodic, patch structured perfect absorber constitutes a compact design concept. The proposed absorber can be applied in solar thermal energy harvesting and photo detection devices.

References

[1] H. T. Chen, J. F. O'Hara, A. K. Azad, A. J. Taylor, Laser Photon. Rev. **5**(4), 513 (2011).

[2] C. M. Watts, X. Liu, W. J. Padilla, Adv. Mater. **24**(23), OP980 (2012).

[3] A. Isenstadt, J. Xu, Electron Mater Lett. **9**(2), 125 (2013).

[4] Y. A. Akimov, K. Ostrikov, E. P. Li, Plasmonics, **4**(2), 107 (2009).

[5] M. B. Pu, Q. Feng, C. G. Hu, X. G. Luo, Plasmonics **7**(4), 733 (2012).

[6] J. W. Park, P. V. Tuong, J. Y. Rhee, K. W. Kim, W. H. Jang, E. H. Choi, L. Y. Chen, Y. P. Lee, Optics Express **21**(8), 9691 (2013).

[7] J. J. Yu, H. J. Chen, X. N. Yu, S. Y. Liu, Chin. Opt. Lett. **12**(s1), S11301-1 (2014).

[8] Z. Z. Li, C. Y. Luo, G. Yao, J. Yue, J. Ji, J. Q. Yao, F. R. Ling, Chin. Opt. Lett. **14**(10), 102303-1 (2016).

[9] J. Hao, J. Wang, X. Liu, W. J. Padilla, L. Zhou, M. Qiu, Appl. Phys. Lett. **96**(25), 251104-1 (2010).

[10] M. A. Kats, D. Sharma, J. Lin, P. Genevet, R. Blanchard, Z. Yang, M. M. Qazilbash, D. N. Basov, S. Ramanathan, F. Capasso, Appl. Phys. Lett. **101**(22), 221101-1 (2012).

[11] T. Cao, C. W. Wei, R. E. Simpson, L. Zhang, M. J. Cryan, Sci. Rep. **4**, 3955 (2014).

[12] W. Wang, S. Wu, K. Reinhardt, Y. Lu, S. Chen, Nano. Lett. **10**(6), 2012 (2010).

[13] K. Aydin, V. E. Ferry, R. M. Briggs, H. A. Atwater, Nat. Commun. **2**, 517 (2011).

[14] H. Ko, D. H. Ko, Y. Cho, I. K. Han, Appl. Phys. A: Mater. Sci. Process **116**(3), 857 (2014).

[15] D. Shrekenhamer, W. R. Xu, S. Venkatesh, D. Schurig, S Sonkusale, W. J. Padilla, Phys. Rev. Lett. **109**(17), 177401-1 (2012).

[16] N. Liu, M. Mesch, T. Weiss, M. Hentschel, H. Giessen, Nano Lett. **10**(7), 2342 (2010).

[17] Y. Wang, T. Y. Sun, T. Paudel, Y. Zhang, Z. F. Ren, K. Kempa, Nano Lett. **12**(1), 440 (2012).

[18] Y. X. Cui, K. H. Fung, J. Xu, H. J. Ma, Y. Jin, S. L. He, N. X. Fang, Nano Lett. **12**(3), 1443 (2012).

[19] M. G. Nielsen, A. Pors, O. Albrektsen, S. I. Bozhevolnyi, Optics Express **20**(12), 13311 (2012).

[20] M. W. Song, H. L. Yu, C. G. Hu, M. B. Pu, Z. J. Zhang, J. Luo, X. G. Luo, Optics Express **21**(26), 32207 (2013).

[21] G. V. Naik, J. Kim, A. Boltasseva, Opt. Mater. Express **1**(6), 1090 (2011).

[22] G. V. Naik, J. L. Schroeder, X. Ni, A. V. Kildishev, T. D. Sands, A. Boltasseva, Opt Mater Express **2**(4), 478 (2012).

[23] G. V. Naik, V. M. Shalaev, A. Boltasseva, Adv. Mater. **25**(24), 3264 (2013).

[24] W. Li, U. Guler, N. Kinsey, G. V. Naik, A. Boltasseva, J. Guan, V. M. Shalaev, A. Kildishev, Adv. Mater. **26**(47), 7959 (2014).

[25] J. G. Wang, W. L. Zhang, M. P. Zhu, K. Yi, J. D. Shao, **10**(6), 1473 (2015).

[26] M. Abb, B. Sepúlveda, M. H. Chong, O. L. Muskens, J. Optics **14**(11), 114007-1 (2012).

[27] S. Rajak, M. Ray, J. Optics, **43**(3), 231 (2014).

[28] A. Taflove, S. C. Hagness, Computational Electrodynamics: the Finite-Difference Time-Domain Method, 3rd Edn., Artech House, 67 (2005).

[29] A. Elsherbeni, V. Demir, The Finite-Difference Time-Domain Method for Electromagnetics with MATLAB Simulations, SciTech Publishing, Inc., 16 (2009).

[30] E. D. Palik, Handbook of Optical Constants of Solids, Academic, 303 (1985).

[31] K. V. Rottkay, M. Rubin, N. Ozer, Mater. Res. Soc. Symp. Proc. **403**, 551 (1995).

[32] F. Miyamaru, M. W. Takeda, Phys. Rev. B **79**(15), 153405-1 (2009).

[33] M. Schwind, B. Kasemo, I. Zorić, Nano Lett. **13**(4), 1743 (2013).

[34] X. Y. Duan, S. Q. Chen, W. W. Liu, H. Cheng, Z. C. Li, J. G. Tian, J. Opt. **16**(12), 125107 (2014).

[35] H. A. Macleod, Thin Film Optical Filters. 4th Edn. (CRC Press) 12 (2010).

[36] N. V. Rottkay, T. J. Richardson, M. Rubin, J. Slack, E. Masetti, G. Dautzenberg, Proc. SPIE **3138**, 9 (1997).

[37] J. Wang, C. Fan, P. Ding, J. He, Y. Cheng, W. Hu, G. Cai, E. Liang, Q. Xue, Opt. Express **20**(14), 14871 (2012).

*Corresponding author: wjg@siom.ac.cn